

České vysoké učení v Praze
Fakulta jaderná a fyzikálně inženýrská

Czech Technical University in Prague
Faculty of Nuclear Sciences and Physical Engineering

Michal Šumbera, CSc., DSc.

Extrémní stavy jaderné hmoty

Extreme states of nuclear matter

Summary

Nuclear matter under extreme temperatures and densities provides a tool to study how collective phenomena and macroscopic properties, involving many degrees of freedom, emerge from the microscopic laws of elementary-particle physics. The most striking case of a collective bulk phenomenon affecting crucially our current understanding of both the structure of the Standard Model and of the evolution of the early universe are the phase transitions between different states of nuclear matter. Experiments with ultra-relativistic nuclei conducted at Relativistic Heavy Ion Collider in New York and at Large Hadron Collider in Geneva have brought astonishing results providing evidence that the hottest ($T > 2 \times 10^{12}\text{K}$) and the most dense nuclear ($\rho > 5 \times 10^{15}\text{gcm}^{-3}$) matter ever created in the laboratory behaves as almost perfect liquid. Resulting shift of the paradigm from long thought weakly interacting gas of quarks and gluons towards the concept of strongly interacting plasma provides an unexpected links to several fields of contemporary physics.

Shrnutí

Jaderná hmota při extrémních teplotách a hustotách umožňuje studovat jak z mikroskopických zákonů fyziky elementárních částic vznikají kolektivní jevy a makroskopické vlastnosti soustav s mnoha stupni volnosti. Nejvíce pozoruhodným příkladem kolektivního jevu ovlivňujícího zásadním způsobem naše současné chápání struktury Standardního modelu a vývoje ranného vesmíru jsou fázové přechody mezi různými stavy jaderné hmoty. Experimenty s ultrarelativistickými jádry prováděné na urychlovačích RHIC v New Yorku a LHC v Ženevě přinesly překvapivé výsledky svědčící o tom, že nejžhavější ($T > 2 \times 10^{12}\text{K}$) a nejhustší ($\rho > 5 \times 10^{15}\text{gcm}^{-3}$) jaderná hmota jakou se kdy podařilo v laboratorních podmínkách připravit se chová jako téměř ideální kapalina. Výsledný posun v paradigmatu od dlouho uvažovaného slabě interagujícího plynu kvarků a gluonů ke konceptu silně interagujícího plazmatu přináší nečekaná spojení s několika moderními fyzikálními obory.

Klíčová slova:

Ideální kapalina, jaderná fyzika vysokých energií, kvark–gluonové plazma, LHC, ranný vesmír, RHIC

Keywords:

Early universe, high energy nuclear physics, ideal liquid, LHC, quark–gluon plasma, RHIC

Contents

1	Introduction	1
2	Theoretical Basis	2
2.1	Phases of nuclear matter	2
2.2	Strongly interacting plasma	4
2.3	Color glass condensate	6
2.4	Transport models	7
3	High energy nuclear physics	9
3.1	History	10
3.2	Flow	11
3.3	Femtoscscopy	14
4	Conclusions	16
5	References	17

1 Introduction

In early hours of 7th November 2010 first lead-lead collisions were seen by the ALICE, ATLAS and CMS experiments at the Large Hadron Collider (LHC) at CERN, Geneva. The big machine has finally delivered its long awaited fruits. The most extreme states of nuclear matter available in the universe only for first few micro seconds after the Big Bang were ready to be studied under laboratory conditions.

Within few weeks of lead ion running first results emerged [1]-[5]. The medium created in Pb-Pb collisions at LHC was found to be very opaque. The most energetic partons emerging from elementary hard collision with momenta exceeding 100 GeV/c are sometimes completely dissipated [5]. The strongly interacting medium produced in Pb-Pb collisions at $\sqrt{s_{NN}}=2.76$ TeV shows features (see Fig. 1) very similar, sometimes even identical to those observed for the first time in $\sqrt{s_{NN}}=200$ GeV Au-Au collisions at Relativistic Heavy Ion Collider (RHIC) at BNL, New York [6]. Similarly to RHIC the hot and dense matter created at the LHC behaves as a nearly perfect liquid [7] and not as a gas of weakly interacting quarks and gluons. This quality becomes even more striking taking into account the latest RHIC measurements performed at c.m.s. energy 70× smaller than the LHC energy. Same function $v_2(p_t)$ shown in the left panel in Fig. 1 describes the data down to $\sqrt{s_{NN}}=39$ GeV [8] extending the regularity over enormous interval of energies. Below this energy the universality is violated [8].

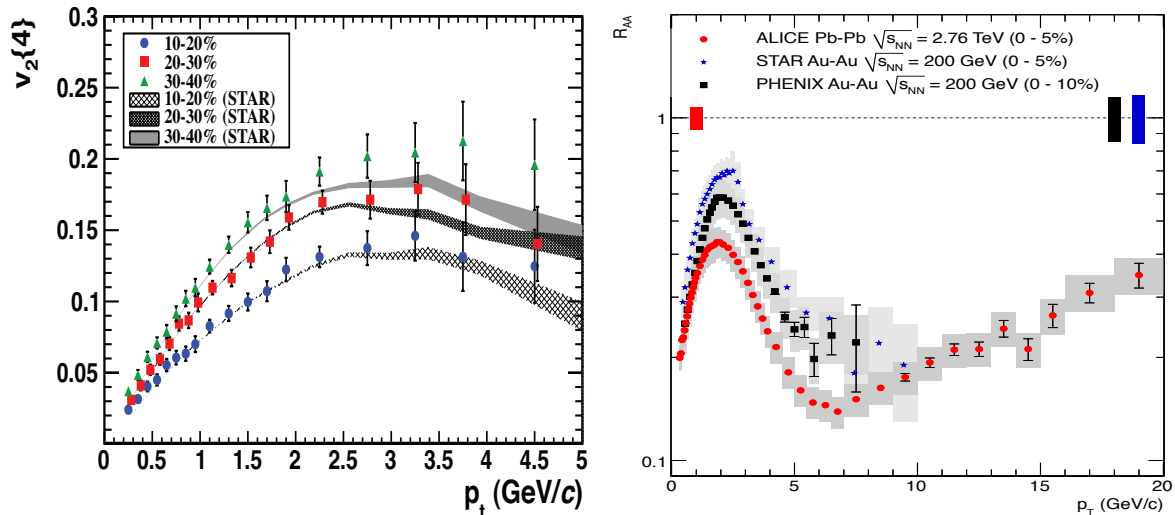


Figure 1: Left: Second harmonic coefficient v_2 of the azimuthal distribution of charged particles w.r.t. the reaction plane as a function of particle transverse momentum p_t at 10-20%,20-30% and 30-40% most central Pb-Pb (Au-Au) collisions [2]. The data points are from LHC, lines correspond to RHIC measurements. Right: $R_{AA}(p_T)$, the ratio of inclusive charged hadron yields in A-A (either Pb-Pb or Au-Au) collisions to p-p, corrected for trivial geometric effects via scaling by $\langle N_{bin} \rangle$, the calculated mean number of binary nucleon-nucleon collisions contributing to given A-A centrality [3].

Are the high energy nuclear collisions at RHIC and LHC trying to tell us something very profound about the early history of the universe [9]? How it will change if the interactions in the medium remain strong close the temperature of the electroweak phase transition[10]? The aim of this lecture is to review history, current status and some open questions of this field of science studying extreme states of nuclear matter.

2 Theoretical Basis

2.1 Phases of nuclear matter

The known matter appears in a variety of phases, which can be transformed into each other by modifying external conditions. Transitions between the phases are often accompanied by a dramatic change in their physical properties, such as density, heat conductivity, light transmission etc.[11]. A famous example is water where changes in external pressure and temperature result in a rich phase diagram (see the left panel of Fig.2). In addition to well understood liquid and gaseous phases plentiful spectrum of solid phases exists in which the H_2O molecules arrange themselves in spatial lattices of certain symmetries. Famous points in the phase diagram are the triple point where the solid, liquid and gas phases coexist and the critical point (T_c, p_c) where no distinction between the liquid and gas phase can not be found. For $T > T_c$ and $p > p_c$ transition between two phases proceeds as a crossover i.e. without traversing any phase boundary.

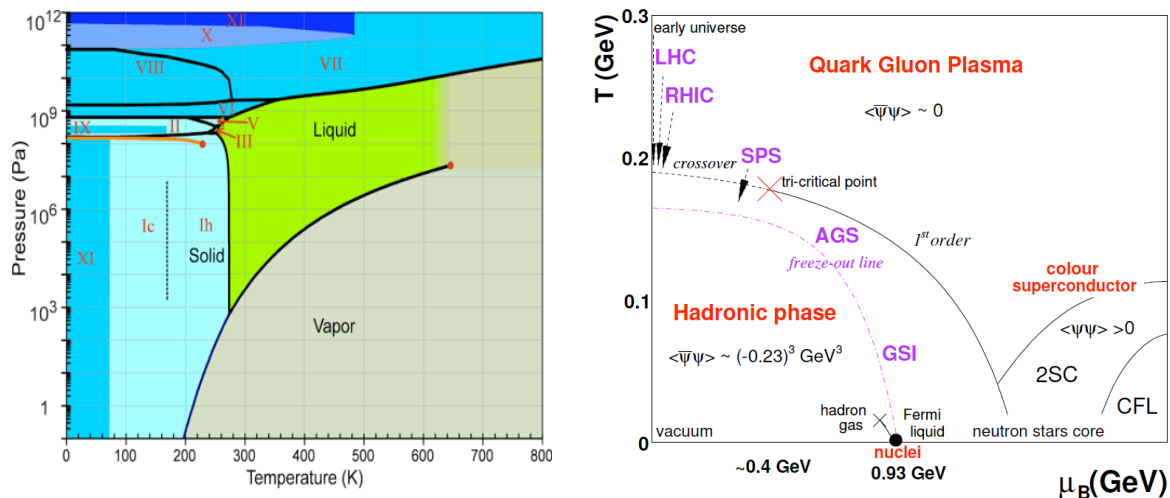


Figure 2: Left: The phase diagram of water [12]. Right: The QCD phase diagram in the temperature vs. baryon chemical potential (T, μ_B) plane [64]. The arrows indicate the expected crossing through the de-confinement transition during the expansion phase in heavy-ion collisions at different accelerators. The (dashed) freeze-out curve indicates where hadro-chemical equilibrium is attained in the final stage of the collision. The ground-state of nuclear matter at $T = 0$ and $\mu_B = 0.93$ GeV and the approximate position of the QCD critical point at $\mu_B \approx 0.4$ GeV are also indicated.

During the evolution of the universe several particle physics related transitions took place [9]. The Standard Model of particle physics (SM) predicts two such transitions [10]. One transition occurs at temperatures of a few hundred GeV. This transition is responsible for the spontaneous breaking of the electroweak (EW) symmetry giving the masses to elementary particles. This transition is also related to the EW baryon-number violating processes, which had a major influence on the observed baryon-asymmetry of the universe. Lattice results have shown that the EW transition in the SM is an analytic crossover [13].

The second transition [14] happens at $T < 200$ MeV and is related to the spontaneous breaking of the chiral symmetry of Quantum Chromodynamics (QCD) – micro-

scopic theory of strong nuclear force responsible for interactions between quarks and gluons. Shortly after discovery of asymptotic freedom of QCD by Gross, Wilczek [15] and Politzer [16], two groups [17, 18] realized independently that when temperatures or densities become very high, strongly interacting quarks and gluons become free and transform themselves into a new, de-confined phase of matter. For the latter the term quark-gluon plasma (QGP) was introduced [19].

Let us note that before discovery of the asymptotic freedom of QCD history of the universe and its composition at temperatures $T \geq m_\pi$ posed big theoretical problems [20]. The reason was thermodynamics of hadronic matter. Increasing temperature of hadronic gas in a fixed volume produces two effects. First, new hadrons are produced increasing rapidly gas density above the limiting value of $n_c \propto 1/V_h = 3/2n_0$, where $n_0 = 0.17 fm^{-3}$ is the normal nuclear matter density and $V_h \approx (4\pi/3)r_h^3$ is a space volume occupied by a single hadron with radius $r_h = 1 fm$. At densities higher than n_c it does not make much sense to speak about the individual hadrons. Second, abundant production of new hadronic species with higher and higher masses occurs. Hagedorn's ingenious approach to relativistic strongly interacting gas problem was to postulate [21] that this gas is a mixture of infinite number of ideal relativistic gases. Component with mass m then contributes to the mixture with weight $\rho(m)$. Experimentally for $m \leq 2 GeV$ the increase of particle spectrum was found to rise like: $\rho(m) \propto exp(bm)$. Although the exponential mass spectrum appeared first in the statistical bootstrap model, based on self-similar resonance formation or decay [21] it was recently found also in finite temperature QCD lattice calculations [22].

Partition function $Z^\rho(T, V)$ of hadronic gas can be then written as an integral over partition function $Z(T, V, m)$ of ideal relativistic gas with mass m :

$$Z^\rho(T, V) = exp\left[\frac{VT}{2\pi^2} \int_0^\infty Z(T, V, m)\rho(m)dm\right], \quad Z(T, V, m) = exp\left[\frac{VT}{2\pi^2} m^2 K_2\left(\frac{m}{T}\right)\right] \quad (1)$$

Let us note that the partition function $Z^\rho(T, V)$ is not defined for all temperatures. Expanding the modified Bessel function $K_2(m/T) \approx (T/m)^{1/2} \times exp(-m/T)$ at $m/T \gg 1$ and plugging it into (1) we see that for $T > T_c = 1/b$ the integral in (1) diverges providing us with a kind of a limiting temperature T_c above which the hadronic gas does not exist. Description of the universe at $T > T_c$ and hence at earlier times is thus impossible [20].

Stimulated by asymptotic freedom discovery Cabbibo and Parisi provided soon the argument against this discouraging result showing that the exponentially increasing mass spectrum is not necessarily connected with a limiting temperature, but it is present in any system which undergoes a second order phase transition [18]. For the particular case of hadronic gas the exponential character of spectrum is connected to the existence of a different phase of the vacuum in which quarks are not confined.

The nature of hadron-to-QGP phase transition affects substantially our understanding of the universe's evolution [10]. For instance in a strong first-order phase transition the QGP supercools before bubbles of hadron gas are formed. Since the hadronic phase is the initial condition for nucleosynthesis [9] the inhomogeneities in this phase could have a strong effect on nucleosynthesis [10]. Knowing that typical baryon chemical potentials are much smaller than the typical hadron masses ($\mu_B \approx 45 MeV$ at RHIC [6] and negligible in the early universe) we can use QCD lattice calculations performed

at $\mu_B = 0$. The results [14, 23] provide a strong evidence that also the QCD transition is a crossover, and thus the above mentioned scenarios – and many others – are ruled out. Numerical simulations on the lattice also indicate that at $\mu_B \approx 0$ MeV the two phase transitions which are possible in the QCD – deconfining and chiral symmetry restoring – occur at essentially the same point [24].

Situation at $\mu_b \gg 0$ MeV and $T \gg 0$ MeV is more complicated (see the right panel of Fig.2). Here the wealth of novel QCD phases is predicted to exist [25]. At $T \approx 0$ MeV and $\mu_B \geq 1$ GeV a variety of color superconducting phases occur. Somewhere on the phase boundary at $\mu_B \approx 400$ MeV critical point separating first and second order phase transition is predicted [25]. Experimental program [26] to find this critical point is now underway at RHIC [8].

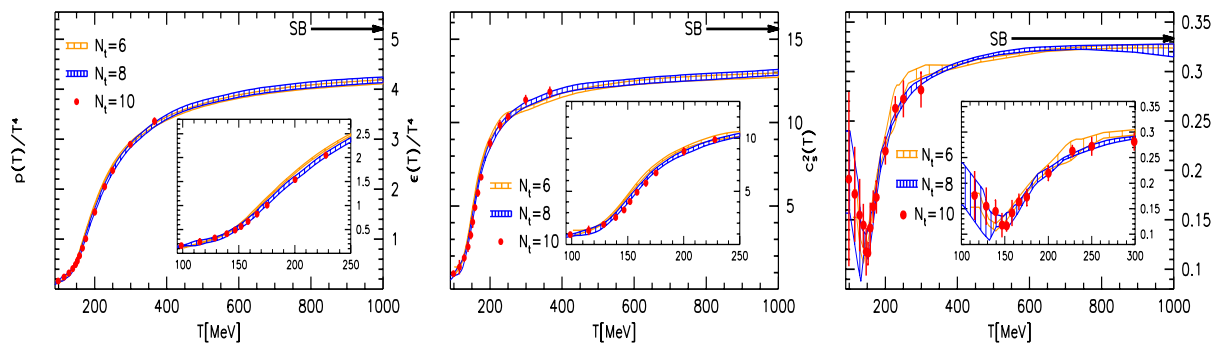


Figure 3: The pressure (left) and energy density (center) normalized by T^4 and the squared of the speed of sound c_s^2 as a function of temperature in QCD with two light and one heavier (strange) quark [23]. The calculations were performed for lattice sizes $N_t = 6, 8$ and 10 . The arrows on the right-side ordinates show the value of the SB limit (2) of the ideal quark-gluon gas.

2.2 Strongly interacting plasma

The properties of QCD equation of state (EOS) with $\mu_B = 0$ are shown on Fig.3 where pressure p and energy density ε normalized to T^4 together with the speed of sound squared $c_s^2 = dp/d\varepsilon$ are plotted as a function of temperature T . The non-perturbative numerical Monte Carlo calculations of QCD thermodynamics employing spacetime discretized onto a lattice [27] was used [23]. Plotting p/T^4 and ε/T^4 instead of p and ε provides a convenient way to display effective number of degrees of freedom g contributing at given temperature T . Hadron gas to QGP phase transition then shows up as an order of magnitude change in p and ε between the pion gas ($g = 3$ corresponds to the three charge states of the pion) and the QGP. Fig.3 shows that the change occurs in a narrow range of temperatures $\Delta T \approx 10 - 20$ MeV around $T \approx T_c \approx 160$ MeV. Since pressure (energy density) is a slowly (rapidly) varying function of T across the critical point T_c , the sound velocity drops down suddenly around $|T - T_c| < \Delta T$. This effect, called 'softening' of EOS, is clearly visible in the inset in Fig.3 right.

Let us note that if the deconfined phase would comply with the original expectations [17] and behave as a gas of weakly interacting quarks and gluons with $N_c = 3$ colors

and $N_f = 3$ quark flavors, the Stefan-Boltzmann (SB) limit:

$$\frac{p}{T^4} = g \frac{\pi^2}{90}, \quad \frac{\varepsilon}{T^4} = g \frac{\pi^2}{30}, \quad g = 2(N_c^2 - 1) + \frac{7}{2} N_c N_f = 47.5 \quad (2)$$

would be reached soon after the phase transition. This is at variance with the lattice QCD calculations shown on Fig.3. p/T^4 rises rapidly above T_c , then begins to saturate by about $2T_c$, but at values substantially below the SB limit indicating substantial remaining interactions among the quarks and gluons in the QGP phase. Let us note that this behavior is completely different from weakly interacting electromagnetic plasma where the SB limit is achieved quite rapidly: $(p - p_{SB})/T^4 \sim T^{-9/2}$ [28].

Let us note that it was not these theoretical calculations but the correct interpretation [29] of experimental data [6] which led to the fall of 30 years old paradigm of weakly interacting QGP controlled by perturbative QCD (pQCD) and to the rise of a new one based on strongly coupled Quark–Gluon Plasma (sQGP) [29, 30]. The basis was the observation that collisions of ultra-relativistic heavy ions produce a flowing medium [2, 6, 7]. This is illustrated on Figs.1, 4, 7 and 8 which will be discussed later on. Let us note that collective flow behavior which persists up to the highest available energies is in complete disagreement with expectations that asymptotic freedom will lead to the weakening of interactions in the QGP.

By definition, plasmas are states of matter in which charged particles interact via long range (massless) gauge fields [30]. This distinguishes them from neutral gases, liquids or solids in which the inter-particle interaction is of short range. So plasmas themselves can be gases, liquids or solids depending on the value of plasma parameter Γ which is the ratio of interaction energy to kinetic energy of the particles forming the plasma [31]. Let us note that strongly coupled classical electromagnetic plasmas $\Gamma > 1$, are not exotic objects at all [31]. For example, table salt NaCl can be considered a crystalline plasma made of permanently charged ions Na^+ and Cl^- [30]. At $T \approx 10^3$ K (still too small to ionize non-valence electrons) it transforms into a molten salt, which is a liquid plasma with $\Gamma \approx 60$. Current estimate of this parameter for the sQGP at RHIC energies $\Gamma = 1.5 - 6$ [32] corresponds also to the liquid plasma.

fluid	p [Pa]	T [K]	η [Pa.s]	η/n [\hbar]	η/s [\hbar/k_B]
H_2O	$0.1 \cdot 10^6$	370	$2.9 \cdot 10^{-4}$	85	8.2
^4He	$0.1 \cdot 10^6$	2.0	$1.2 \cdot 10^{-6}$	0.5	1.9
H_2O	$22.6 \cdot 10^6$	650	$6.0 \cdot 10^{-5}$	32	2.0
^4He	$0.22 \cdot 10^6$	5.1	$1.7 \cdot 10^{-6}$	1.7	0.7
^6Li ($a = \infty$)	$12 \cdot 10^{-9}$	$23 \cdot 10^{-6}$	$\leq 1.7 \cdot 10^{-15}$	≤ 1	≤ 0.5
QGP	$88 \cdot 10^{33}$	$2 \cdot 10^{12}$	$\leq 5 \cdot 10^{11}$		≤ 0.4

Table 1: Viscosity η , viscosity over density η/n and viscosity over entropy density η/s ratio for several fluids at particular values of pressure p and temperature T , from [35].

Very promising strongly interacting plasmas which can be studied in the laboratory are strongly coupled ^6Li atoms and graphene [33]. Distinctive property of these plasmas is that, similarly to the QGP, their shear viscosity to entropy density ratio η/s characterizing how close is the fluid to a perfect liquid [34] is effectively negligible [30, 35].

Cold atomic gases are produced in optical or magneto-optical traps [36]. These traps typically contain $10^5 - 10^6$ atoms. Hydrodynamic behavior is observed when the trapping potential is modified, or if the local density or energy density is modified using laser beams. In this way the scattering length a (and hence the interaction strength between the atoms) can be made almost infinite [30]. This is also the case of data point ${}^6\text{Li}$ ($a = \infty$) shown in the Table 1 where the thermodynamical parameters for several other substances of interest is summarized. For H_2O and ${}^4\text{He}$ two points are displayed. First are the data at atmospheric pressure and temperatures just below the boiling point and the λ transition, respectively. These data points roughly correspond to the minimum of η/n at atmospheric pressure. Second are the data near the critical point which roughly corresponds to the global minimum of η/s .

2.3 Color glass condensate

Another phenomenon where the quarks and gluons can not be treated as independent is a case of parton coherence. Generalization of pQCD to hard collisions of small- x ($x \ll 1$) partons were first discussed by Gribov, Levin and Ryskin [37]. They tried to cure the inconsistency of the standard approach which predicts too fast increase of small- x partons density with Q^2 . Consequently, the growth of hadronic cross sections proceeds at rate which would sooner or later violate the unitarity. Proposed solution – parton recombination and saturation – is at variance with standard assumption that the partons themselves can be considered as an independent free particles. The parameter determining the probability of parton–parton recombination is the ratio of the parton–parton cross section to the square of the average distance between partons. The fact that cross section of such semi-hard process (which now complies with the unitarity) increases rapidly with incident energy gives rise to expectations that (at least asymptotically) the bulk particle production in hadron-hadron collisions can be described via pQCD [29].

A modern implementation of the above ideas is the Color Glass Condensate (CGC) formalism [38] – natural generalization of the pQCD to dense partonic systems. When applied to heavy nuclei it predicts strong color fields in the initial stage of the collision. The strength of the fields is due to condensation of low- x gluons into single classical field state – the Color Glass Condensate. Since characteristic scale of the parton saturation grows as $Q_s \propto A^{1/3}$ [29, 38] it is enhanced on nuclear targets. According to the CGC motivated phenomenology the saturation phenomena are expected to show up already in p-Au or d-Au collisions at RHIC [41].

Supporting argument for the CGC as a possible state of QCD matter came from the analysis of HERA data in terms of Geometrical Scaling (GS) [39]. GS is the statement that the total γ^*p cross section depending a priori on two independent variables – the photon virtuality Q^2 and the Bjorken variable x is only function of a single variable $\tau = Q^2/Q_s^2$. saturation scale Q_s^2 depends nontrivially on x , with dimensions given by a fixed reference scale Q_0^2 . However, recent calculation [40] shows that the standard linear leading-order DGLAP perturbative evolution is able to explain the geometric scaling. Situation with CGC applicability is thus unsettled. Experimental data from RHIC and LHC as well as exploitation of non-CGC based models [42] are needed to resolve this problem.

Another look at the multiparton phenomena comes from the study of forward-backward multiplicity correlations among the hadrons produced in collisions of two heavy ultra-relativistic nuclei [43]. Contrary to p-p collisions where only short-range correlations are present the multiple parton interactions may produce large long-range correlations extending beyond ± 1 units in rapidity. One mechanism to produce the long-range correlations could be the CGC induced Glasma produced in the early stages of heavy ion collision [44]. However, a very similar prediction comes also from parton and hadron cascade calculations [45].

2.4 Transport models

One of the main tasks of the theory is to link experimental observables to the different phases and manifestations of the QCD matter. To achieve this goal, a detailed understanding of the dynamics of heavy ion reactions is essential. This is facilitated by transport theory which helps to interpret or predict the quantitative features of heavy ion reactions. It is particularly well suited for the non-equilibrium situation, finite size effects, non-homogeneity, N-body phase space, particle/resonance production and freeze-out as well as for collective dynamics. Microscopic [46]-[48] and macroscopic (hydrodynamical) [49]-[51] transport models attempt to describe the full time-evolution from the initial state of the heavy ion reaction up to the freeze-out of all initial and produced particles after the reaction.

Hadronic cascade models, some with mean-field interactions, have succeeded in reproducing the gross and many detailed features of the nuclear reactions measured at Dubna Synchrophasotron [52] and GSI SIS [46, 47, 53, 54]. They have become indispensable for experimentalists who wish to identify interesting features in their data or to make predictions to plan new experiments. The general success of these models at lower energies can nonetheless easily lead to misconceptions at higher energies. The main concern is the relevancy of these models at high particle densities which are so characteristic for collisions of heavy systems. Here all the models based on hadronic dynamics are fundamentally inconsistent [55]. Studying how big is the fraction of the energy contained in known hadrons and that one temporarily stored in a more elusive objects, such as pre-hadronized strings, it was found [47] that up to a time of 8 fm/c most of the energy density resides in strings and other high-mass continuum states that have not fully decayed. Physical properties of these objects are poorly known even when they occur in isolation [56], not to speak about their interactions (or even their existence) in a dense environment. The application of these models to the early phase of collision of two ultra-relativistic heavy nuclei is therefore ill-founded [55].

The idea to use the laws of ideal hydrodynamics to describe the expansion of the strongly interacting matter formed in high energy hadronic collisions was first formulated by Landau in 1953 [57]. Later on Bjorken [58] discovered a simple scaling solution that provides a natural starting point for more elaborate solutions in the ultra-relativistic domain. The phenomenological success of Landau model was for decades big challenge to high energy physics [59]. First because hydrodynamics is a classical theory, second that it assumes local equilibrium. Both these assumptions imply a large number of degrees of freedom and it is by no means clear that the highly excited, but still small systems produced in violent nuclear collisions satisfy the criteria justifying treatment in terms of a macroscopic theory [50]. Therefore the Landau model (and

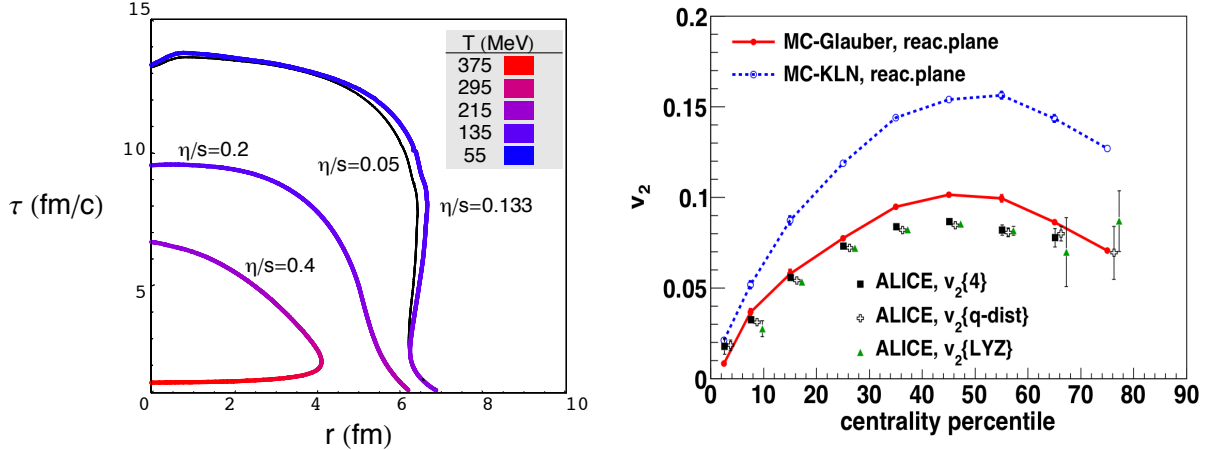


Figure 4: Left: Location of freeze-out surfaces for central Au-Au collisions [35]. Right: Centrality dependences of elliptic flow of charged hadrons from Pb-Pb collisions at $\sqrt{s_{NN}} = 2.76$ TeV [63]. ALICE data are from [2].

other statistical models of strong interactions) were considered up to the mid-seventies as exotic approaches, outside mainstream physics [59]. Then the authors of [60]-[62] realized that exploitation of hydrodynamics in the interpretation of data is the only chance of proving in the laboratory the existence of a new state of matter. This is a trivial corollary of the well known fact that a state of matter is defined by its EOS, and there is no other way to get information about the EOS than by using the hydrodynamics [49, 50, 59].

The complementarity between microscopic and macroscopic description becomes obvious for the case of strongly interacting plasmas. The fact that for liquids neither Boltzmann equation nor cascades can be used stems from the fact that particles are strongly correlated with several neighbors at all times. The very idea of “scattering” and cross section involves particles coming from and going to infinity: it is appropriate for dilute gases but not condensed matter where interparticle distances do not exceed the range of the forces at any time [30].

Fig. 4 provides two examples of transport models calculations. The left panel shows location of freeze-out surfaces for central Au-Au collisions at several fixed values of the shear viscosity to entropy density ratio η/s obtained from numerical solution of viscous hydrodynamics [35]. The shading corresponds to the freeze-out temperature. Freeze-out occurs when the viscous terms become large compared to the ideal terms. Note that hydrodynamics breaks down not only at late but also at early times (see the curve $\eta/s=0.4$ on Fig. 4). The right panel displays centrality dependence of the elliptic flow coefficient v_2 (Eq. (3)) on initial density in the transverse plane – one motivated by the parton saturation (CGC) other exploiting nucleons only (Glauber). The calculations [63] were done within a hybrid model where the expansion of the QGP starting at $\tau_0=0.6$ fm/c is described by ideal hydrodynamics with a state-of-the-art lattice QCD EOS, and the subsequent evolution of hadronic matter below switching temperature $T_{sw} = 155$ MeV, is described using a hadronic cascade model. This nicely illustrates the strength of hydrodynamics – either the QGP viscosity of from RHIC to LHC increases or the CGC initial condition is ruled out [63].

3 High energy nuclear physics

High energy nuclear physics (HENP) studies nuclear matter in energy regimes delegated until recently to particle physics only (see Fig.5, left). Aim of this new field of science [67, 71] is to apply and extend the Standard Model of particle physics to complex and dynamically evolving systems of finite size. Its primary goal is to study and understand how collective phenomena and macroscopic properties, involving many degrees of freedom, emerge from the microscopic laws of particle physics. The most striking case of a collective bulk phenomenon affecting crucially our current understanding of both the structure of the SM at low energy and of the evolution of the early universe are the phase transitions in quantum fields at characteristic energy densities [10]. HENP thus fulfills part of the important mission of nuclear science – to explain the origin, evolution, and structure of the baryonic matter of the universe.

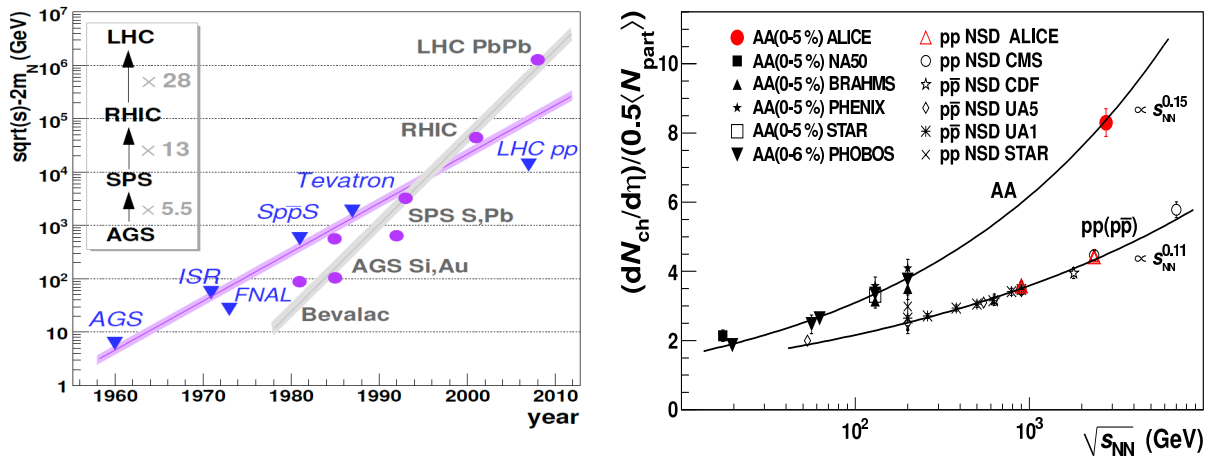


Figure 5: Left: 'Livingston plot' for (anti)proton and ion accelerators in the period 1960- 2008 [64]. Right: Charged particle pseudo-rapidity density per participant pair for central nucleus–nucleus and non-single diffractive pp/pp collisions, as a function of the c.m.s. energy per nucleon-nucleon pair $\sqrt{s_{NN}}$ [1].

The evolution of the accelerators available for HENP experiments and example illustrating one basic measurement are illustrated on Figs. 5. On the left panel maximum c.m.s. energy available for production of new particles $\sqrt{s} - 2m_N$ in nucleus–nucleus (A-A) or nucleon–nucleon (N-N) collisions available at given accelerator as a function of the year of its inauguration is plotted.

On the right panel of Fig.5 charged-particle pseudo-rapidity density per participant pair $(dN_{ch}/d\eta)/\langle N_{part} \rangle$ is plotted as a function of energy. This is the first step in characterizing similarity/difference between A-A and N-N collisions. When A-A collision proceeds as a simple superposition of free p-p interactions one expects this quantity to be the same for both types of collisions. Experimental results on Fig.5 invalidate this assumption. Moreover, for A-A collisions a stronger energy dependence is observed – $s_{NN}^{0.15}$ compared to $s_{NN}^{0.11}$ for pp/pp collisions – reflecting different interplay between hard and soft processes in A-A and N-N collisions. $dN_{ch}/d\eta$ thus not only constrains the dominant particle production mechanisms but it is also essential for estimate of the initial energy density [58]. We will see later on that $dN_{ch}/d\eta$ alone determines evolution of several final state observables in A-A collisions.

3.1 History

The basic hopes and goals, associated with investigations of heavy ion collisions were first formulated in mid-seventies [60, 61, 66]. It was the experience with astrophysical objects like supernovae and neutron stars, and with thermonuclear ignition, which led the authors to an idea that nuclear matter shock compression of about five-fold normal nuclear density should be accomplished in violent head-on collisions of heavy nuclei [67]. The goal was to find out the response of the nuclear medium under compression by pressure resisting that compression, i.e. to study the nuclear matter equation of state (EOS). The original question was: is such a bulk nuclear matter EOS accessible within the dynamics of relativistic heavy ion collisions? [68]. The prospect to observe phase transition at highly compressed nuclear matter [69] was lurking behind.

The interest in collisions of high-energy nuclei as a possible route to a new state of nuclear matter was substantially strengthened with the emergence of QCD. Since mid-seventies the particle physics community began to adapt existing high-energy accelerators to provide heavy-ion nuclear beams (see the left panel of Fig.7). The Berkeley Bevalac and JINR Synchrophasotron started to accelerate nuclei to kinetic energies from few hundreds of MeV to several GeV per nucleon [67, 68]. By the mid-1980s, the first ultra-relativistic nuclear beams became available. Silicon and gold ions were accelerated to 10 GeV/nucleon at Brookhaven's Alternating Gradient Synchrotron [67].

At CERN the first nuclear collisions took place in early eighties when alpha particles were accelerated to $\sqrt{s_{NN}} = 64$ GeV at the ISR collider. The proposal by L. van Hove [70] and few others to continue this programme using heavy nuclei was rejected, the experiments never went beyond the alpha-particles, and then this first hadronic collider was disassembled. As we know now, QGP could have been discovered and studied at ISR 20 years prior to RHIC [30].

The new era of HENP begun in fall 1986 when oxygen and later on in summer 1990 sulphur ions were injected into the at CERN SPS and accelerated to energy of 200 AGeV ($\sqrt{s_{NN}} = 19.6$ GeV) [67]. However, genuine heavy ion programe started only in 1994, after the CERN accelerator complex has been upgraded with a new lead ion source which was linked to pre-existing, interconnected accelerators, the Proton Synchrotron (PS) and the SPS [71, 72]. The seven large experiments – NA44, NA45/CERES, NA49, NA50, NA52, WA97/NA57 and WA98 – have started to study different aspects of Pb-Pb and Pb-Au collisions at $\sqrt{s_{NN}} = 17.2$ GeV and $\sqrt{s_{NN}} = 8.6$ GeV. First, essentially circumstantial evidence about the QGP, was announced by CERN in February 2000 [72].

In the meantime at Brookhaven National Laboratory (BNL) the Relativistic Heavy Ion Collider rose up from the ashes of the ISABELLE/CBA $\bar{p}p$ collider project abandoned by the particle physicist in 1983. In 1984 the first proposal for the dedicated nucleus-nucleus machine accelerating gold nuclei up to $\sqrt{s_{NN}} = 200$ GeV was submitted. Funding to proceed with the construction was received in 1991. On June 12th, 2000 first Au-Au collisions at $\sqrt{s_{NN}} = 130$ GeV were recorded by the BRAHMS, PHENIX, PHOBOS and STAR experiments [29]. The following three years have witnessed a plethora of interesting, sometimes even unexpected, results [6].

The idea of the Large Hadron Collider dates back even further – to the early 1980s. Although CERN's Large Electron Positron Collider (LEP), which ran from 1989 to 2000, was not built yet, scientists considered re-using the 27-kilometer LEP ring for an

even more powerful p-p machine. The LHC was designed to run at highest possible collision energies $\sqrt{s} = 14$ TeV and intensities. The ion option ($\sqrt{s_{NN}} = 5.4$ TeV per nucleon-nucleon pair for Pb-Pb collisions) was considered since the beginning. The LHC was approved in December 1994, its official inauguration took place in October 2008 at CERN. First p-p collisions at $\sqrt{s} = 900$ GeV were observed on November 23rd, 2009. Energy $\sqrt{s} = 3.5$ TeV was reached on March 30th, 2010. First Pb-Pb collisions at $\sqrt{s_{NN}} = 2.76$ TeV were recorded on November 7th, 2010. In the following weeks a spectacular phenomena confirming, besides others, the previous RHIC discoveries were reported [1]-[5].

3.2 Flow

Let us start a short review of experimental results with a bulk phenomenon which is driving this field for the last two decades [49, 67, 74]. In non-zero impact parameter ($b > 0$) collisions of two nuclei the overlap region is not azimuthally symmetric (see Fig. 6, right). Its almond shape manifests itself in reaction plane defined by the direction of the impact parameter and the direction of the beam axis. It is customary to quantify particle emission with respect to the reaction plane using Fourier coefficients v_n :

$$E \frac{d^3 N}{dp^3} = \frac{1}{2\pi} \frac{d^3 N}{p_T dp_T dy} \left[1 + \sum_n 2v_n \cos(n\phi) \right] \quad (3)$$

where the reaction plane is approximated by the vector $\vec{Q} \equiv \sum_\nu w_\nu \vec{p}_T(\nu)$. Here $p_T(\nu)$ is the transverse momentum and w_ν an appropriately chosen weight for the individual particle in an event. The azimuthally symmetric coefficient v_0 is called transverse radial flow. v_1 and v_2 are called directed and elliptic flow, respectively.

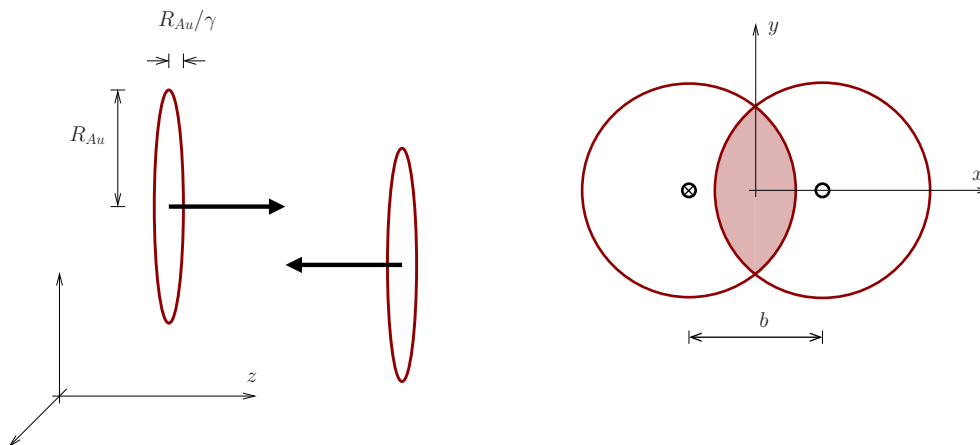


Figure 6: Geometry of a high energy heavy ion collision. Left: Collision of two Lorentz contracted gold nuclei. The beam direction is the z -axis. Right: the same but in the transverse plane. The impact parameter is along the x -axis, and the remaining transverse direction is the y -axis.

The elliptic flow affects all final state particles and so in contrast to many other early fireball signatures, it can be easily measured with high statistical accuracy. The beam energy dependence of the elliptic flow of charged particles is displayed on the left panel of Fig.7. At very low energies, due to the rotation of the compound system

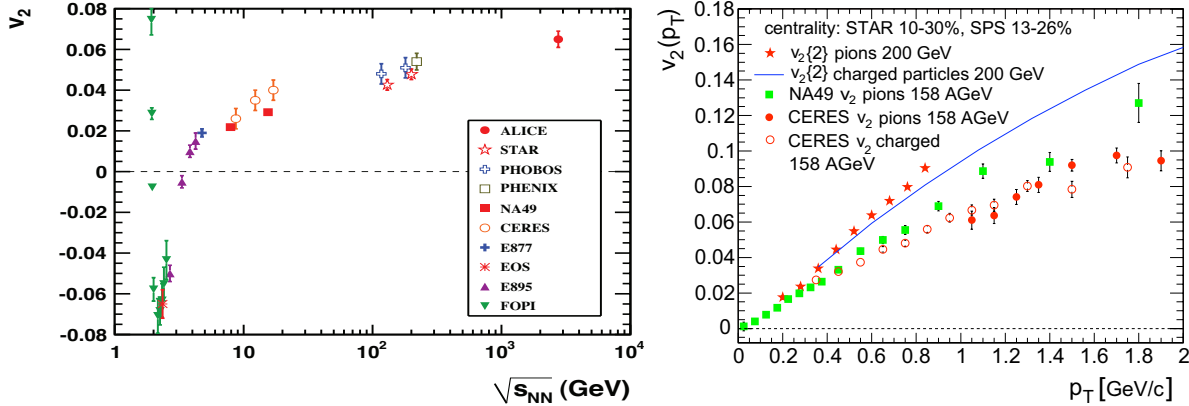


Figure 7: Left: Energy-dependence of elliptic flow v_2 (near midrapidity, integrated over p_T) for semi-central collisions of Pb or Au nuclei [2]. Right: $v_2(p_T)$ for one centrality (10-30%) range. The circles and squares are results from the SPS experiments at $\sqrt{s_{NN}} = 17.2$ GeV. The stars and the solid line are STAR measurements for pions and for all charged particles, respectively, at $\sqrt{s_{NN}} = 200$ GeV [6].

generated in the collision, the emission is in-plane ($v_2 > 0$). At the laboratory kinetic energy around 100 MeV/nucleon, the preferred emission turns into out-of-plane and v_2 becomes negative. Since the slowly moving spectator matter prevents the in-plane emission of participating nucleons or produced pions they appear to be squeezed-out of the reaction zone [73]. As the spectators move faster at Lorentz $\gamma \geq 3$ ($E_{beam} \approx 6$ GeV/nucleon) this shadowing disappears changing the pattern back to the in-plane emission. Above this energy v_2 increases monotonically up to the highest energies.

As was first noted by Ollitrault [74] at high energies only the interactions among the constituents of the matter formed in initially spatially deformed overlap can produce $v_2 > 0$. Transfer of the spatial deformation into the momentum space provides a unique signature for re-interactions in the fireball and proves that the matter has undergone significant nontrivial dynamics between its creation and its freeze-out [50]. Rapid degradation of the initial spatial deformation is due to re-scattering and causes the ‘self-quenching’ of elliptic flow: if elliptic flow does not develop early, when the collision fireball was still spatially deformed, it does not develop at all [50]. Elliptic flow thus reflects the pressure due to re-scattering-induced expansion and stiffness of the equation of state during the earliest collision stages [30]. Its continuous rise up to its highest value at the LHC indicates that the early pressure increases too.

Let us note that at RHIC for the first time the magnitude of radial and elliptic flow was found to be consistent with EOS expected from the QGP [6, 50, 71]. The integrated value of v_2 for the produced particles increases by 70% from the top SPS energy to the top RHIC energy (see the left panel of Fig.7), and it appears to do so smoothly. The origin of this energy dependence can be determined by examining the differential $v_2(p_T)$, shown for the centrality selection 10–30% on the right panel of Fig. 7. The comparison of the results for pions at $\sqrt{s_{NN}} = 200$ GeV and at the top SPS energy $\sqrt{s_{NN}} = 17.2$ GeV reveals an increase in slope of $v_2(p_T)$ that accounts for part of the increase in p_T -integrated v_2 . The remaining part of the change is due to the increase in $\langle p_T \rangle$. This indicated that at RHIC hadronic degrees of freedom are unable to account for the early formation of significant pressure leading to explosive

collective behavior [30]. Since near to a phase transition the EOS becomes very soft (see Fig.3, right) preventing the generation of flow [30] the anisotropic flow production is concentrated to even earlier times, when the system is still entirely partonic and has not even begun to hadronize [50]. At highest RHIC energy this means that almost all of the finally observed elliptic flow is created during the first 3–4 fm/c [6].

Contrary to this between RHIC and LHC $v_2(p_T)$ does not change at all (Fig.1, left). As already mentioned in the Introduction energy dependence of $v_2(p_T)$ is saturated starting already from $\sqrt{s_{NN}}=39\text{GeV}$ [8]. The rise of the integrated elliptic flow value in this energy range is due solely to the increase in $\langle p_T \rangle$.

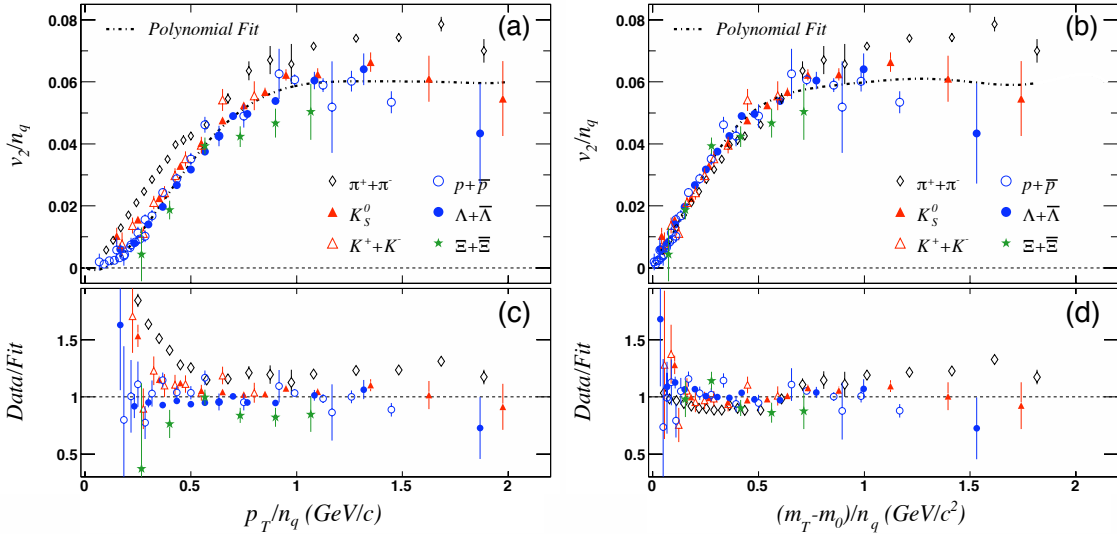


Figure 8: Identified particle v_2 from minimum bias collisions at $\sqrt{s_{NN}} = 62.4$ GeV scaled by the number of valence quarks in the hadron (n_q) and plotted versus p_T/n_q (a) and $(m_T - m_0)/n_q$ (b). In each case a polynomial curve is fit to all particles except pions. The ratio of v_2/n_q to the fit function is shown in the bottom panels (c) and (d). [75]

On Fig.8(a) the RHIC data on elliptic flow of identified particles from Au+Au minimum-bias sample are presented in such a way that both v_2 and p_T are divided by the number of valence quarks n_q in the hadron of interest ($n_q=2$ or 3 for mesons and baryons, respectively). The apparent scaling behavior seen on the figure is intriguing, as the data themselves seem to be pointing to constituent quarks (or at least to valence quarks sharing the full hadron momentum) as the most effective degree of freedom determining flow of hadrons. The scaling becomes almost perfect when replacing p_T by the transverse kinetic energy $\sqrt{p_T^2 + m_0} - m_0$ (Fig.8(b)).

In [76] it is argued that the QGP-to-hadron chiral phase transition does not result at once in the formation of the ordinary hadronic matter. Instead a specific and quite long-lived phase occurs in which pions and kaons are the only hadron species that can survive. They stay in chemical and thermal equilibrium with the deconfined phase composed of the massive constituent quarks. The second phase transition occurs when the substance becomes so rarefied that the color-screening length (approximately equal to the mean spacing of constituent quarks) becomes equal to the confinement radius.

Though the constituent quarks are not part of QCD Lagrangian they were repeatedly suggested as a viable degrees of freedom of the effective QCD field theory [77, 78].

3.3 Femtoscopy

Progress in understanding the space-time structure of multiparticle production via momentum correlations of two or more particles at small relative momenta [79] – called nowadays the correlation femtoscopy [80] – is driven by high-statistics data accumulated in heavy ion experiments at LHC, RHIC and SPS [4, 6, 82, 83]. In particular, an ambitious program of the STAR collaboration at RHIC exploiting good particle identification has already provided a vast variety of femtoscopic results in different identical and non-identical particle systems, some of which were actually measured for the first time [82]. The measurements exploit the large final-state density of mesons, baryons and their antiparticles leading sometimes even to the first class discovery like that of antimatter hypernucleus [84].

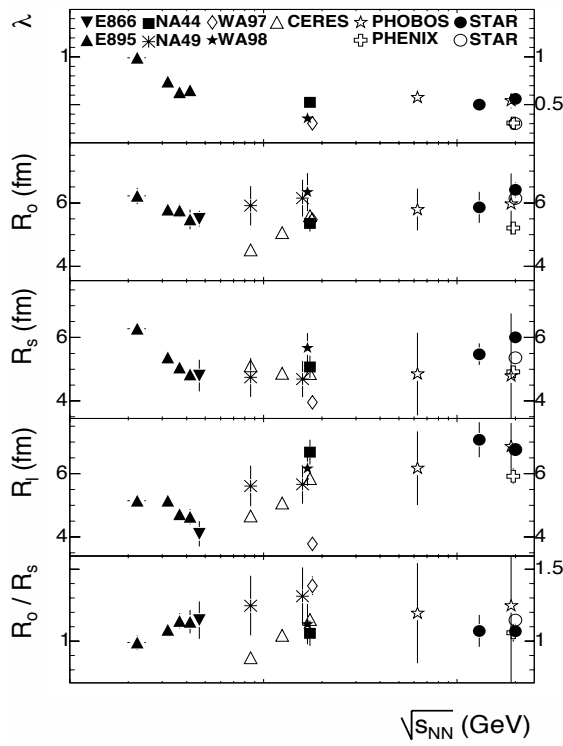


Figure 9: Energy dependence of HBT parameters extracted from pion pair correlations in central A+A ($A = 200$) collisions at mid-rapidity and pair $k_T \approx 0.2$ GeV/c [6].

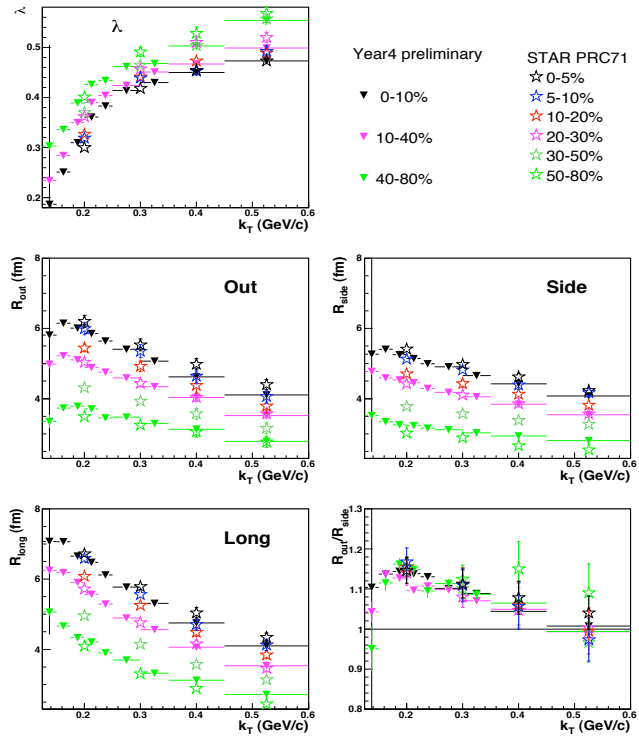


Figure 10: k_T -dependence of the radii R_{out} , R_{side} , R_{long} extracted from the correlation functions of identical charged pions from Au+Au collisions at $\sqrt{s_{NN}}=200$ GeV [82].

World summary on identical pion pair correlations is shown in Fig.9. The displayed parameters were extracted from a three-dimensional Gaussian parametrization of the correlation function of identical pions $C_2(\vec{q})$ [79], splitting the three-momentum difference vector \vec{q} into a longitudinal and two transverse components $\vec{q} = (q_{long}, q_{side}, q_{out})$. The out-component is parallel to the pair transverse momentum and side perpendicular to the other two. Fitting this parametrization to the data yields the correlation strength λ and the radii R_{long} , R_{side} and R_{out} shown in Fig.9.

Like most of the bulk properties measured at RHIC [6] the emitting source radii appear to fall on quite smooth curve with similar results from lower-energy collisions.

Moreover, the energy dependence of the radii can be transformed into approximately linear dependence on $(dN_{ch}/d\eta)^{1/3}$ [4, 79] where $dN_{ch}/d\eta$ is the midrapidity charged particle density. These experimental results contrast with theoretical speculations and predictions made before the RHIC start-up [67], which often suggested [70, 85] strong energy dependences accompanying the hadron-to-QGP phase transition. The observed smooth general behavior has been primarily attributed to the formation of matter over a range of initial local conditions, even at a given collision energy or centrality, and to the absence of any direct experimental determination of early temperature [50]. In any case, the results clearly highlight the difficulty of observing any rapid 'smoking-gun' onset of a transition to a new form of matter [6].

Despite this smoothness, two important milestones related to the attainment of thermal equilibrium appear to be reached at RHIC [6]. The yields of different hadron species, up to and including multi-strange hadrons, become consistent with a grand canonical statistical distribution at a chemical freeze-out temperature of 163 ± 5 MeV and a baryon chemical potential ≈ 25 MeV. This result sets an effective lower limit on the temperatures attained if thermal equilibration is reached during the collision stages preceding this freeze-out. This lower limit is essentially equal to the QGP transition temperature predicted by the lattice QCD calculations [14, 24] (see Fig. 3).

Second, for near-central RHIC collisions the mass- and p_T -dependence of the observed hadron spectra [6] and of the strong elliptic flow (see Figs. 1 and 7) in the soft sector become consistent, at the ± 20 -30% level, with hydrodynamic expectations for an ideal relativistic fluid formed with an initial eccentricity characteristic of the impact parameter [30, 72]. These hydrodynamic calculations have been for a long time rather unsuccessful in explaining quantitatively the emitting hadron source size inferred from the measured femtoscopic correlations [79, 80]. This failure, which became known as the HBT puzzle, now appears to be solved [81]. The discrepancy appears to be due to several factors – pre-equilibrium flow, a stiffer equation of state and non-zero viscosity – each of which contributed to making the evolution of RHIC collisions more explosive.

Fig.10 shows results from the STAR experiment [82] on dependence of the radii R_{long} , R_{side} and R_{out} on the average transverse momentum of the pion pair k_T . Characteristic fall-off of the pion source radii with k_T showing up at all centralities is due to a collective hydrodynamic-like flow [79, 80]. In the absence of space-momentum correlations all source parameters would be k_T -independent.

Both longitudinal and radial collective expansion reduce the size of the 'region of homogeneity', i.e., the relevant volume for particles of a given velocity. In particular the magnitude of the longitudinal size of the pion source is in a boost-invariant scenario [58] determined by the interplay between the thermal motion and the longitudinal expansion: R_{long} is the z-range over which the thermal velocity $v_{therm} \sim \sqrt{T/m_t}$ can compensate the Bjorken collective expansion velocity $v_{exp} = z/t$ such that two particles emitted at different z-coordinates can still have similar momenta. The resulting (Makhlin-Sinyukov) formula [79] $R_{long} = \tau_f \sqrt{T/m_t}$ describes characteristics k_T -dependence of R_{long} and also dependence of its magnitude on the total duration of the longitudinal expansion τ_f and the temperature T .

On Fig.11 the latest femtoscopic results [4] from the ALICE experiment at LHC are compared to the previous heavy ion measurements. The product of the radii $R_{out}R_{side}R_{long}$, which is connected to the volume of the homogeneity region, shows a

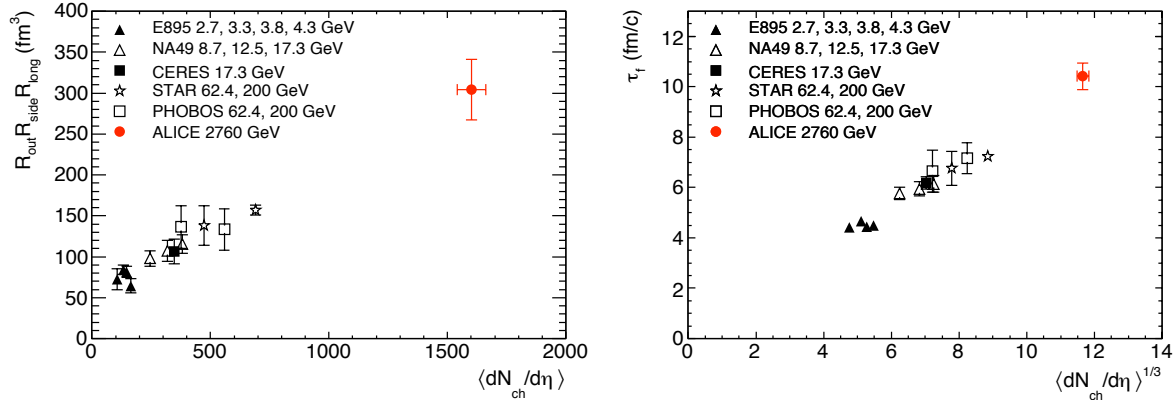


Figure 11: Left: Product of the three pion HBT radii at $k_t = 0.3\text{GeV}/c$ as a function of charged particle density $\langle dN_{ch}/d\eta \rangle$. Right: The decoupling time τ_f extracted from $R_{long}(k_t)$ as a function of $\langle dN_{ch}/d\eta \rangle^{1/3}$. The ALICE result is compared to central gold and lead collisions at lower c.m.s. energies. From [4].

linear dependence on the charged particle density $\langle dN_{ch}/d\eta \rangle$ and is two times larger at the LHC than at RHIC. Moreover, similarly to the radii R_{out} , R_{side} and R_{long} the total duration of the longitudinal expansion τ_f also rises linearly with $\langle dN_{ch}/d\eta \rangle^{1/3}$. These results, taken together with those obtained from the study of multiplicity [1] (Fig.5, right) and the azimuthal anisotropy [2] (Figs. 1, left and 4, right), indicate that the fireball formed in nuclear collisions at LHC is indeed hotter, lives longer, and expands to a larger size at freeze-out as compared to lower energies [4].

4 Conclusions

The program to study high-density nuclear matter was formulated a long time ago [60, 61, 66, 69]. At about that time the new phase of QCD matter – deconfined and chirally symmetric QGP – was predicted to exist [17, 18]. First, essentially circumstantial evidence about the QGP, came from the CERN SPS experiments [72]. The result was based on combination of several observed signals (strangeness enhancement, J/ψ suppression, dilepton and direct photon production) each of them allowing also for a non-QGP explanation.

Soon after the CERN QGP announcement the RHIC machine started to deliver its first results. The following years have witnessed a plethora of interesting, sometimes unexpected, results [6, 41, 43, 71, 75]. The first RHIC data have confirmed that the magnitude of observed collective phenomena is consistent with equation of state expected from the QGP. Hadronic degrees of freedom are unable to account for the early formation of significant pressure leading to explosive collective behavior [50]. The non-trivial properties of the matter created at RHIC were also found in the region where according to standard wisdom pQCD calculations should be valid: large deficit of high- p_T hadrons (the jet quenching), large (and approximately p_T -independent) azimuthal asymmetry and baryon/meson ratio much larger than in the usual jet fragmentation. In the meantime the matter with similar properties was also found at the LHC [1]-[5].

The extreme state of nuclear matter studied at RHIC and LHC exhibits unique and

an hithero unexpected behavior. Collisions of ultra-relativistic nuclei produce very high density, strongly interacting matter (made of constituent quarks), reaching very early the thermal equilibrium [2, 6]. Surprisingly enough, the super-dense matter does not behave as the ideal gas of free quarks and gluons – a subject of intensive search in previous decades – but manifest itself as a perfect fluid [30, 50, 29]. Another phase of nuclear matter – hypothetical Color Glass Condensate – is still beyond the experimental reach.

5 References

- [1] K. Aamodt . . . , M. Šumbera *et al.*(ALICE Coll.), Phys. Rev. Lett. **105**, 252301 (2010).
- [2] K. Aamodt,. . . , M. Šumbera *et al.*(ALICE Coll.), Phys. Rev. Lett. **105**, 252302 (2010).
- [3] K. Aamodt,. . . , M. Šumbera *et al.* (ALICE Coll.), Phys. Lett. **B696**, 30 (2011).
- [4] K. Aamodt,. . . , M. Šumbera *et al.* (ALICE Coll.), Phys. Lett. **B696**, 328 (2011).
- [5] G. Aad *et al.* (Atlas Coll.), Phys. Rev. Lett. **105**, 252303 (2010).
- [6] J. Adams,. . . , M. Šumbera *et al.* (STAR Coll.), Nucl. Phys. A **757**, 102 (2005).
- [7] B. Jacak, P. Steinberg, Phys. Today **63N5**, 39-43 (2010).
- [8] L. Kumar for the STAR Collaboration, arXiv:1101.4310 [nucl-ex].
- [9] S. Weinberg, *Cosmology*, Oxford Univ. Press, 2008, ISBN 978-0-19-852682-7.
- [10] D. Boyanovsky, H. J. de Vega, D. J. Schwarz, Ann. Rev. Nucl. Part. Sci. **56**, 441 (2006).
- [11] P. M. Chaikin, T. C. Lubensky, *Principles of condensed matter physics*, Cambridge University Press, 1995, ISBN 0-521-43224-3.
- [12] M. Chaplin, *Water Structure and Science*, <http://www.lsbu.ac.uk/water/phase.html>.
- [13] K. Kajantie *et al.*, Phys. Rev. Lett. **77**, 2887 (1996).
- [14] Y. Aoki, G. Endrodi, Z. Fodor, S. D. Katz and K. K. Szabo, Nature **443**, 675 (2006).
- [15] D. J. Gross and F. Wilczek, Phys. Rev. Lett. **30** (1973) 1343.
- [16] H. D. Politzer, Phys. Rev. Lett. **30** (1973) 1346.
- [17] J. C. Collins and M. J. Perry, Phys. Rev. Lett. **34**, 1353 (1975).
- [18] N. Cabibbo and G. Parisi, Phys. Lett. B **59** (1975) 67.
- [19] E. V. Shuryak, Sov. Phys. JETP **47**, 212 (1978) [Zh. Eksp. Teor. Fiz. **74**, 408 (1978)].
- [20] K. Huang and S. Weinberg, Phys. Rev. Lett. **25** (1970) 895.
- [21] R. Hagedorn, Nuovo Cim. Suppl. **3**, 147 (1965).
- [22] A. Majumder, B. Muller, Phys. Rev. Lett. **105**, 252002 (2010).
- [23] S. Borsanyi, G. Endrodi, Z. Fodor *et al.*, JHEP **1011**, 077 (2010).
- [24] M. Cheng *et al.*, Phys. Rev. D **77**, 014511 (2008).
- [25] K. Fukushima, T. Hatsuda, Rept. Prog. Phys. **74**, 014001 (2011).
- [26] M. M. Aggarwal, . . . , M. Šumbera *et al.* (STAR Coll.), arXiv:1007.2613 [nucl-ex].
- [27] D. E. Miller, Phys. Rept. **443**, 55 (2007).
- [28] L. D. Landau, E. M. Lifshitz, *Statistical Physics, Part 1. Vol. 5 (3rd ed.)*. Butterworth-Heinemann. ISBN 978-0-750-63372-7.
- [29] M. Gyulassy and L. McLerran, Nucl. Phys. A **750**, 30 (2005).
- [30] E. Shuryak, Prog. Part. Nucl. Phys. **62**, 48 (2009).
- [31] S. Ichimaru, Rev. Mod. Phys. **54**, 1017 (1982).
- [32] M. H. Thoma, J. Phys. G **31**, L7 (2005),
- [33] C. V. Johnson, P. Steinberg, Phys. Today **63N5**, 29 (2010).
- [34] P. Kovtun, D. T. Son, A. O. Starinets, Phys. Rev. Lett. **94**, 111601 (2005).
- [35] T. Schafer, D. Teaney, Rept. Prog. Phys. **72**, 126001 (2009).
- [36] J. E. Thomas, Phys. Today **63N5**, 34 (2010).
- [37] L. V. Gribov, E. M. Levin and M. G. Ryskin, Phys. Rept. **100**, 1 (1983).
- [38] J. Jalilian-Marian and Y. V. Kovchegov, Prog. Part. Nucl. Phys. **56**, 104 (2006).

- [39] K. J. Golec-Biernat and M. Wusthoff, Phys. Rev. D **60**, 114023 (1999).
- [40] F. Caola and S. Forte, Phys. Rev. Lett. **101**, 022001 (2008).
- [41] J. Adams, . . . , M. Šumbera *et al.* (STAR Coll.), Phys. Rev. Lett. **97**, 152302 (2006).
- [42] J. Nemchik and M. Šumbera, Nucl. Phys. A **830**, 611c (2009)
- [43] B. I. Abelev, . . . , M. Šumbera *et al.* (STAR Coll.), Phys. Rev. Lett. **103**, 172301 (2009).
- [44] T. Lappi and L. McLerran, Nucl. Phys. A **832**, 330 (2010).
- [45] Y.-L. Yan, D.-M. Zhou, B.-G. Dong *et al.*, Phys. Rev. **C81**, 044914 (2010).
- [46] J. Aichelin, Phys. Rept. **202**, 233 (1991).
- [47] S. A. Bass *et al.*, Prog. Part. Nucl. Phys. **41**, 255 (1998).
- [48] K. Werner, Phys. Rept. **232**, 87 (1993).
- [49] H. Stöcker and W. Greiner, Phys. Rept. **137**, 277 (1986).
- [50] U. W. Heinz, arXiv:0901.4355 [nucl-th].
- [51] E. Schnedermann, J. Sollfrank and U. W. Heinz, Phys. Rev. C **48**, 2462 (1993).
- [52] G. S. Shabratova, M. Šumbera, *et al.*, Z. Phys. A **318**, 75 (1984)
- [53] F. D. Berg . . . , M. Šumbera *et al.*, Phys. Rev. Lett. **72**, 977 (1994)
- [54] O. Schwalb . . . , M. Šumbera *et al.*, Phys. Lett. B **321**, 20 (1994)
- [55] B. Muller, Nucl. Phys. A **661**, 272 (1999).
- [56] W. Kittel, E. A. De Wolf, *Soft multihadron dynamics*. World Scientific (2005).
- [57] L. D. Landau, Izv. Akad. Nauk Ser. Fiz. **17**, 51 (1953).
- [58] J. D. Bjorken, Phys. Rev. D **27**, 140 (1983).
- [59] R. M. Weiner, Int. J. Mod. Phys. E **15**, 37 (2006).
- [60] W. Scheid, H. Muller and W. Greiner, Phys. Rev. Lett. **32**, 741 (1974).
- [61] M. I. Sobel, H. A. Bethe, P. J. Siemens, J. P. Bondorf, Nucl. Phys. A **251**, 502 (1975).
- [62] J. J. Griffin and K. K. Kan, Rev. Mod. Phys. **48**, 467 (1976).
- [63] T. Hirano, P. Huovinen, Y. Nara, arXiv:1012.3955 [nucl-th].
- [64] D. G. d’Enterria *et al.*, (CMS Coll.), J. Phys. G **34**, 2307 (2007).
- [65] K. Aamodt, . . . , M. Šumbera *et al.*, (ALICE Coll.), JINST **0803**, S08002 (2008).
- [66] G. F. Chapline, M. H. Johnson, E. Teller and M. S. Weiss, Phys. Rev. D **8**, 4302 (1973).
- [67] R. Stock, in Landolt-Börnstein - Group I Elementary Particles, Nuclei and Atoms, Vol.**21A**, Chapter 7, Springer Berlin Heidelberg,2009. arXiv:0807.1610 [nucl-ex].
- [68] R. Stock, Phys. Rept. **135**, 259 (1986).
- [69] T. D. Lee and G. C. Wick, Phys. Rev. D **9**, 2291 (1974).
- [70] L. Van Hove, Phys. Lett. B **118**, 138 (1982).
- [71] P. Braun-Munzinger and J. Stachel, Nature **448**, 302 (2007).
- [72] U. W. Heinz and M. Jacob, arXiv:nucl-th/0002042.
- [73] L. B. Venema, . . . , M. Šumbera *et al.* (TAPS Coll.), Phys. Rev. Lett. **71**, 835 (1993)
- [74] J. Y. Ollitrault, Phys. Rev. D **46**, 229 (1992).
- [75] B. I. Abelev, . . . , M. Šumbera *et al.* (STAR Coll.), Phys. Rev. **C75**, 054906 (2007).
- [76] I. I. Roizen, E. L. Feinberg, O. D. Chernavskaya, Phys. Usp. **47**, 427 (2004).
- [77] K. G. Wilson *et al.*, Phys. Rev. **D49**, 6720 (1994).
- [78] S. Weinberg, Phys. Rev. Lett. **105**, 261601 (2010).
- [79] M. A. Lisa *et al.*, Ann. Rev. Nucl. Part. Sci. **55**, 357 (2005).
- [80] R. Lednický, Nucl. Phys. A **774**, 189 (2006).
- [81] S. Pratt, Nucl. Phys. **A830**, 51c (2009).
- [82] M. Šumbera for the STAR Collaboration, Braz. J. Phys. **37**, 925 (2007).
- [83] D. Adamová, . . . , M. Šumbera *et al.*(CERES Coll.), Phys. Rev. Lett. **90**, 022301 (2003).
- [84] B. I. Abelev, . . . , M. Šumbera *et al.* (STAR Coll.), Science **328**, 58 (2010).
- [85] D. H. Rischke and M. Gyulassy, Nucl. Phys. A **608**, 479 (1996).

Michal Šumbera, CSc., DSc.

Born: March 5th, 1951, Prague, Czech Republic
Affiliation: Nuclear Physics Institute, Czech Academy of Sciences
Address: Řež 130, 250 68 Řež, Czech Republic
Email: sumbera@ujf.cas.cz

Research areas

High energy nuclear physics, multiparticle production

Professional carier

2006 - member of the Scientific council of the Faculty of Nuclear Science and Physical Engineering, Czech Technical University, Prague
2003 - member of the Collaboration Council of the STAR experiment at RHIC
1996 - member of the Collaboration Board of the ALICE experiment at LHC
1995 - leader of ultra-relativistic heavy ion group, Nuclear Physics Institute
1993 - Nuclear Physics Institute ASCR, senior scientist
1991 - 1993 Kernfysisch Vernsneeler Instituut, Groningen, The Netherlands, visiting scientist
1984 - 1991 Nuclear Physics Institute ASCR, staff scientist
1978 - 1984 Laboratory of High Energies, Joint Institute of Nuclear Research, Dubna, USSR, staff scientist
1975 - 1978 Nuclear Physics Institute ASCR, scientific associate

Qualification

DSc. in physical-mathematical sciences	2010	Academy of Sciences of the Czech Republic
CSc. (PhD.) in experimental physics	1984	Laboratory of High Energies, JINR, Dubna
MSc. in nuclear and particle physics	1974	Faculty of Mathematics and Physics, Charles University, Prague

Professional activity

- 200 published scientific papers
- Princial investigator in 5 finished and 2 running grant projects
- Organizer of conferences and workshops
- Winner of the JINR annual award competition in 1989

Teaching activity

- taught courses: Extreme States of Matter, Quantum Chromodynamics, Physics of Heavy ion Collisions.
- supervised four defended PhD theses and two defended diploma theses.